The Astrophysical Journal Letters, 927:L2 (5pp), 2022 March 1 https://doi.org/10.3847/2041-8213/ac52ae

Solar Toroidal Field Evolution Spanning Four Sunspot Cycles Seen by the Wilcox Solar Observatory, the Solar and Heliospheric Observatory/Michelson Doppler Imager, and the Solar Dynamics Observatory/Helioseismic and Magnetic Imager

Allison L. Liu[1] and Philip H. Scherrer[2]
[1] Los Gatos High School, Los Gatos, CA 95032, USA; pscherrer@solar.stanford.edu
[2] W. W. Hansen Experimental Physics Laboratory, Stanford University, Stanford, CA 94305-4085, USA
Received 2022 January 16; revised 2022 February 5; accepted 2022 February 8; published 2022 February 28

Abstract

Forty-four years of Wilcox Solar Observatory, 14 years of Michelson Doppler Imager on the Solar and Heliospheric Observatory, and 11 years of Helioseismic and Magnetic Imager on the Solar Dynamics Observatory magnetic field data have been studied to determine the east–west inclination—the toroidal component—of the magnetic field. Maps of the zonal averaged inclination show that each toroidal field cycle begins at around the same time at high latitudes in the northern and southern hemispheres, and ends at the equator. Observation of these maps also shows that each instance of a dominant toroidal field direction starts at high latitudes near sunspot maximum and is still visible near the equator well past the minimum of its cycle, indicating that the toroidal field cycle spans approximately two sunspot cycles. The length of the extended activity cycle is measured to be approximately 16.8 yr.

Unified Astronomy Thesaurus concepts: Solar cycle (1487)

1. Introduction

The solar magnetic field exhibits an activity cycle that can be described by the solar dynamo that converts the solar poloidal magnetic field to the toroidal field and then generates a new poloidal field from the toroidal field (e.g., Cameron et al. 2018). It is manifested by solar sunspots appearing at the Sun's surface that show an 11 yr solar cycle. An extended activity cycle is suggested by several models to predict the coexistence of two consecutive cycles on the Sun (Howard & Labonte 1980; Snodgrass 1985, 1987). The length of the extended activity cycle in these models is predicted to be approximately 22 yr (Howard & Labonte 1980) and approximately 18 yr (Snodgrass 1985), respectively. Detecting and determining the extended activity cycle can help in understanding the solar dynamo, which is fundamental in understanding the Sun's activity evolution.

The extended activity cycle can be detected by several methods (Cameron et al. 2018), including the toroidal magnetic field on the solar surface (Duvall et al. 1979; Ulrich 1993; Shrauner & Scherrer 1994; Ulrich et al. 2002; Ulrich & Boyden 2005; Lo et al. 2010; Cameron et al. 2018). Ulrich & Boyden (2005) found the extended activity cycle in the toroidal field, which is derived from magnetograms from the Mount Wilson Observatory (MWO; Ulrich et al. 2002) from 1984 to 2004. Cameron et al. (2018) calculated the toroidal field from the magnetograms taken at the Wilcox Solar Observatory (WSO; Scherrer et al. 1977) and the Michelson Doppler Imager (MDI; Scherrer et al. 1995) on the Solar and Heliospheric Observatory (SOHO). The toroidal field from both instruments shows the extended activity cycle consistently, even at high latitudes. With a similar method, Shrauner & Scherrer (1994) studied the extended activity cycle by calculating the magnetic field inclination, which is the angle with respect to the radial direction (Duvall et al. 1979), a proxy of the toroidal field. They used 16 yr of WSO magnetograms. The results show an extended cycle with a length of 16–18 yr. The WSO data have low spatial resolution, and the data at high latitudes are very limited. Thus, the data used are within 60° in latitude. The length of the extended cycle can now be determined more accurately with the availability of new data from the MDI and the Helioseismic and Magnetic Imager (HMI; Scherrer et al. 2012) on the Solar Dynamics Observatory (SDO; Pesnell et al. 2012). The higher spatial resolution afforded by MDI and HMI has been used to obtain better measurements at high latitudes. Lo et al. (2010) and Cameron et al. (2018) used MDI data with a span of about 12 yr, not long enough to show a complete extended cycle. Early efforts to add more years with HMI (Ma & Scherrer 2016) were too short to show convincing higher-latitude development.

The purpose of this work is to use magnetogram data collected from three sources, WSO, MDI, and HMI, to examine the existence of an extended activity cycle. The paper is organized as follows. Section 2 describes the method used to calculate the inclination. Processing the observation data of WSO, MDI, and HMI is also described in this section. The results are presented in Section 3. The work is concluded in Section 4.

2. Methodology and Data

2.1. Methodology

The method used in this study was adapted from the method used in Duvall et al. (1979) and Shrauner & Scherrer (1994). Figure 1, similar to Figure 1 in Shrauner & Scherrer (1994), illustrates how the inclination angle (α) is calculated from the observed line-of-sight magnetic field (B_l). Following the rotation of the Sun, a region of interest rotates from the east limb to the west. B_l in the region varies as a function of the

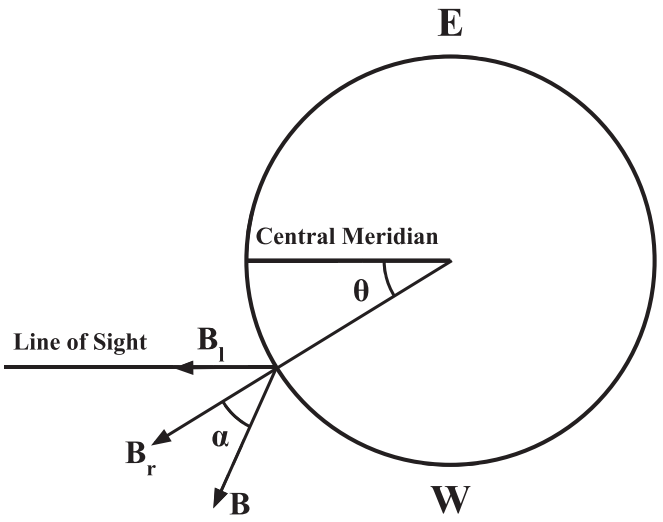

Figure 1. B_l and θ as derived from the solar disk are illustrated in relation to the central meridian and the inclined magnetic field line, B. B_r is the radial field. The figure is adapted from Duvall et al. (1979) and Shrauner & Scherrer (1994).

angle from the central meridian, θ, as

$$B_l(\theta) = B\cos(\alpha + \theta), \tag{1}$$

where B is the magnitude of the magnetic field in the region. Tracking the region from east to west allows us to measure B_l multiple times. These measurements are then used to compute the inclination α by

$$\tan(\alpha) = \frac{\left(\sum_i B_l^i \cos\theta_i\right)\left(\sum_i \sin\theta_i \cos\theta_i\right) - \left(\sum_i B_l^i \sin\theta_i\right)\left(\sum_i \cos^2\theta_i\right)}{\left(\sum_i B_l^i \cos\theta_i\right)\left(\sum_i \sin^2\theta_i\right) - \left(\sum_i B_l^i \sin\theta_i\right)\left(\sum_i \sin\theta_i \cos\theta_i\right)}, \tag{2}$$

where i represents the number of times measured (Shrauner & Scherrer 1994). The inclination angle is defined to be positive in the direction of rotation (westward) and negative in the direction opposite to rotation (eastward). The inclination was computed for positive and negative fields separately.

The inclination is calculated for each and every solar rotation (Carrington Rotation). For each longitude in one Carrington Rotation, the data from individual magnetograms were chosen if the central meridian of the magnetogram was within 55° from the selected longitude. The selected magnetic field data, B_l, and the angle from the central meridian, θ, were applied to Equation (2) to calculate the inclination. Therefore, in the end, we obtained two inclination maps for each Carrington Rotation: one from the positive field and the other from the negative field. The inclination is a positive angle if it tilts toward the direction of rotation, such that sunspots with negative leading and positive following spots contribute to a positive toroidal component. The toroidal field is the difference in the tilts of the positive and negative fields in each coordinate bin. The strength of the toroidal field measured this way will be about the sine of the tilt times the line-of-sight field at the disk center. We have not attempted to do this calibration due to many sources of systematic errors and because the pattern of the changing toroidal field is itself a useful measurement.

2.2. Data

The data used in this research are full-disk line-of-sight magnetograms from WSO, MDI, and HMI. WSO started observations in 1976 and continues to the present day; MDI is from 1996 to 2011, and HMI is from 2010 to the present. The data sizes are 11 × 11 for WSO, 1024 × 1024 for MDI, and 4096 × 4096 for HMI, respectively.

The magnetograms on the image coordinates were first mapped to an equal-area projection on the Carrington heliospheric coordinates for inclination calculation. For the WSO data, the magnetograms were interpolated to 30 steps in sine latitude and 23 steps of 5° in longitude on the spatial grid. We used all the WSO data from 1976 to 2021. The MDI magnetograms were mapped on the heliospheric coordinates with a data size of 1800 × 1440 and further smoothed and resized to 180 × 144. The data cadence of the MDI magnetograms is 96 minutes. In this study, we used one sample every 192 minutes from 1996 to 2010. The HMI magnetograms were processed in the same way. The HMI magnetograms used in the study are obtained every 12 minutes. We used one sample every 180 minutes from 2010 to 2021.

3. Results

3.1. Length of the Extended Activity Cycle

The resulting toroidal field maps from all three sources of data indicate clear patterns in the extended activity cycle, as shown in Figure 2. These maps were obtained by taking the zonal average of the toroidal field for each Carrington Rotation and mapping these averages together as a function of time in years. Figure 2 shows sin(latitude)–time diagrams of the toroidal field from WSO (top) and MDI and HMI (middle), together with the sunspot number with time as a reference (bottom). The sunspot number data are from the Sunspot Index and Long-term Solar Observations at https://wwwbis.sidc.be/silso/infosnmtot. Following Shrauner & Scherrer (1994), for the WSO remapped data, we removed the data at the very top and very bottom rows due to poor data quality. Blue refers to positive toroidal field and red to negative field. A sign change of the toroidal field at high latitude indicates the start of a new cycle, and a sign change at the equator indicates the end of the cycle. The plot shows that the start of a new cycle occurs approximately at the maximum of a sunspot cycle and ends well past the minimum of the next cycle, suggesting an extended activity cycle that is approximately 16–18 yr, which is in agreement with Shrauner & Scherrer (1994). This supports the theoretical suggestion of an extended activity cycle (Howard & Labonte 1980; Snodgrass 1985, 1987). Not only did we obtain an extended activity cycle from WSO data, which was consistent with previous studies (Shrauner & Scherrer 1994; Lo et al. 2010), we also confirmed this result with new data from both MDI and HMI. A clearer trend in high latitudes is evidently revealed from the HMI data.

To find a more quantitative determination of the length of the extended activity cycle, we used the toroidal maps of the WSO data because we have enough WSO data to calculate for multiple extended cycles (top panel in Figure 2). We divided the toroidal field map into multiple horizontal bins at different latitudes and averaged each latitude bin to derive the toroidal field in this latitude as a function of time. We then fitted each averaged data with an 11th order polynomial function, as this order fit the trend the best. With polynomial functions of orders

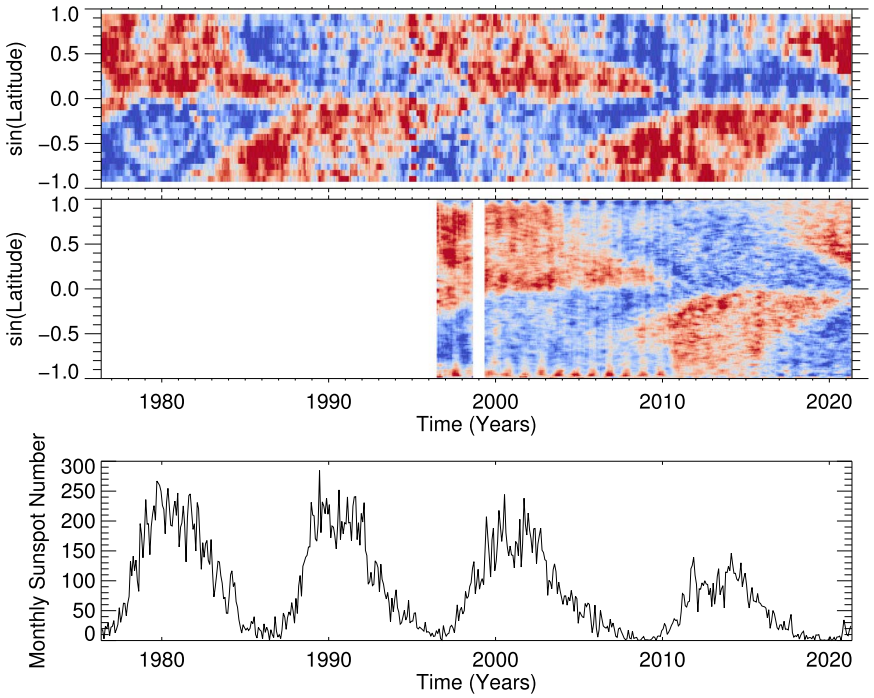

Figure 2. Sin(latitude)–time diagrams of the toroidal fields from WSO (top) and MDI and HMI (middle) data. The temporal profile of the monthly averaged sunspot number is exhibited in the bottom panel. Blue indicates a positive toroidal field in the direction of solar rotation, i.e., westward; red indicates a negative toroidal field in the direction opposite to solar rotation, i.e., eastward.

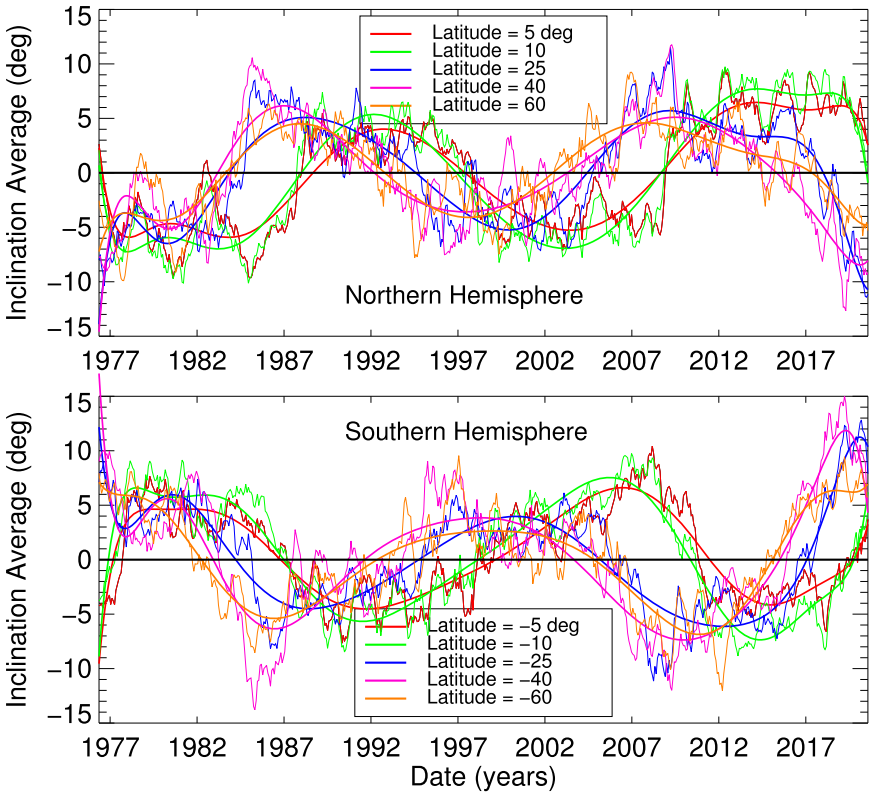

Figure 3. Temporal profiles of toroidal fields at different latitudes for the northern (top) and southern hemispheres (bottom). The irregular, jagged curves with different colors refer to the calculated toroidal fields at different latitudes. The smoothed thicker curves represent the 11th order polynomial functions fitted to the toroidal fields.

lower than 11, the function did not closely fit the overall trend of the averaged data, but a polynomial of a higher order displayed the details in the data that contaminate the trend. Finally, we determined the time the sign changes (i.e., when the sign of the toroidal field changes from positive to negative and vice versa) from the fitted polynomial function. The results are shown in Figure 3. The times of these results are listed in Table 1. Using the data in Table 1, we can measure the time the

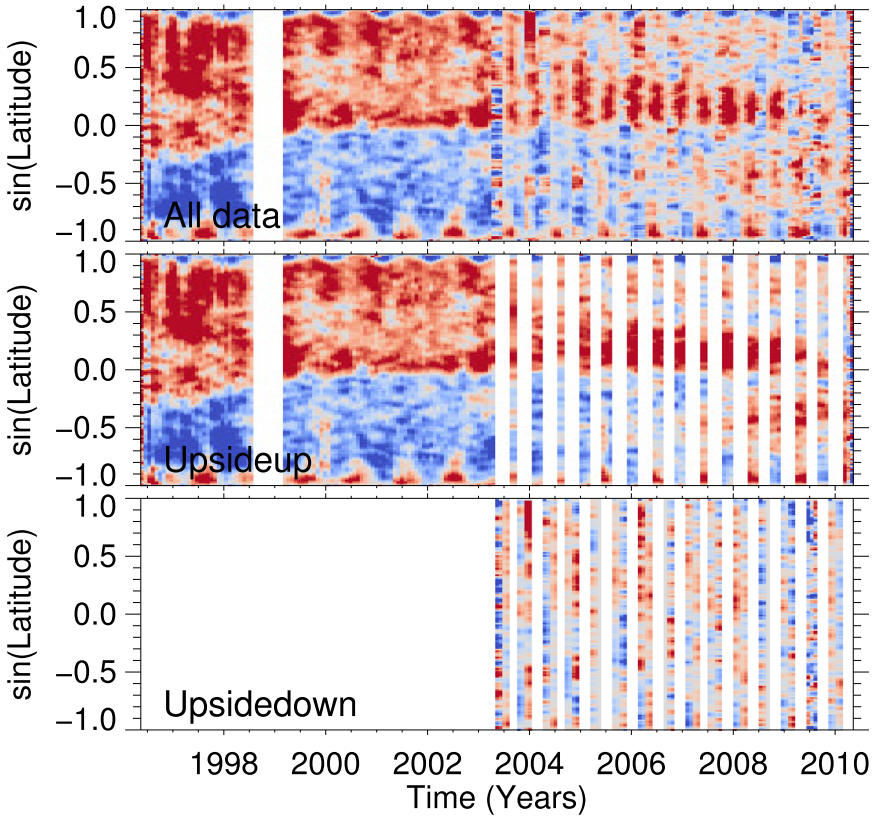

Figure 4. Sin(latitude)–time diagrams of the toroidal fields from MDI data. Top: sin(latitude)–time diagram from all the data. Middle: sin(latitude)–time diagram from upside-up data only. Bottom: sin(latitude)–time diagram from upside-down data only. The pattern becomes much clearer when only upside-up data are used (middle panel) while there is no clear pattern in the upside-down map (bottom panel).

Table 1
Dates of Sign Change of the Toroidal Field versus Latitude from WSO Data

Latitude	1	2	3	4	5
60°	1983.75	1992.92	2002.58	2017.58	
40°	1983.25	1992.25	2003.42	2014.58	
25°	1984.00	1994.67	2004.42	2016.00	
10°	1976.42	1988.08	1997.00	2008.75	2020.50
5°	1976.67	1988.75	1997.75	2008.83	
−5°	1977.17	1986.83	1999.17	2011.50	2017.33
−10°	1977.00	1987.08	1998.25	2010.33	2018.75
−25°	1984.33	1994.83	2005.25	2016.67	
−40°	1983.00	1991.75	2003.75	2014.83	
−60°	1982.33	1992.50	2004.92	2015.17	

sign changes at 5° and 60° in latitude. (For the last cycle, we used the sign-change times at 10° and 60° in latitude.) Subtracting the dates of the sign change at 60° in latitude from the dates of the sign change at 5° in latitudes results in the length of the cycle. For the six complete sections, which we denoted with different colors in Table 1, three in the northern hemisphere and three in the south, the length between the sign change at high latitude and at the equator is about 15.9 yr in the northern hemisphere and 16.6 yr in the southern hemisphere. For all six samples, the mean is 16.2 ± 1.9 yr. This is the lower bound of the length of the extended activity cycle because the data at higher latitudes are missing.

Using the points where the sign changes for each extended cycle (listed in Table 1), we can fit a linear function and then calculate the length of the extended cycle. We applied this method to HMI data only because HMI has better resolution at high latitudes than WSO. Because HMI data are shorter, we were only able to apply a linear fitting to the data for one time of sign change, starting at high latitude at approximately 2015 and at low latitude at approximately 2020. However, to determine the length of an extended solar cycle, we need the data for two consecutive cycles to determine the start and end of the extended cycle. In order to find the linear fitting for the previous times of sign change, we used the linear function that we calculated for the current times of sign change and shifted it parallel to the previous times of sign change. The length between the sign change at the pole and at the equator is about 16.9 yr in the northern hemisphere and 17.7 yr in the southern hemisphere.

The length of the extended activity cycle from three data sources and with different methods generally converges. The visualization of the toroidal field maps from the three data sources yields a length of 16–18 yr, measuring the times of the sign change at 5° and 60° from WSO data gives a length of 16.2 yr, and using a linear function to fit the sign-change times at different latitudes for HMI data leads to a length of 17.3 yr. Further study is needed to measure the length more accurately after more HMI data are collected.

3.2. Questionable MDI Data

While the HMI data show a much clearer pattern of the extended activity cycle, the map from the MDI data looks questionable, with vertical strips after 2003 (see Figure 2). A hardware failure in the SOHO spacecraft in 2003 made it necessary to make observations upside down every other

90 days. The data during this time period may have calibration issues.

We tested this speculation by separating the upside-up and upside-down data and calculated the toroidal field separately. The result is shown in Figure 4, where the toroidal field map from all the MDI data is plotted in the top panel, and the maps from the upside-up and upside-down data are shown in the middle and bottom panels, respectively. The trend becomes much clearer when the upside-down data are excluded (middle panel), while the map from the upside-down data does not show a clear pattern but rather a mixture of signs. Thus, these upside-down data cause the vertical strips seen in the top panel of Figure 4.

4. Conclusion

In this study, we derived the toroidal field, the east–west inclination of the magnetic field, from magnetogram data from WSO, MDI, and HMI, utilizing the method from previous studies (Duvall et al. 1979; Shrauner & Scherrer 1994). We were able to detect a clear pattern of the extended activity cycle that is consistent with previous studies (Shrauner & Scherrer 1994; Lo et al. 2010) not only from WSO data but also from both MDI and HMI data, which confirms the previous findings. Using these methods to process HMI data, we were able to observe the toroidal field detected at high latitudes due to high-resolution data produced by HMI. Using toroidal field maps derived from data from WSO and HMI, we calculated the extended activity cycle and found it to be approximately 16.8 yr, which supports the results of previous studies. Additionally, we observed calibration issues with MDI data when the instrument is upside down.Acknowledgments

We thank the anonymous referee for the valuable suggestions that helped to improve the paper. A.L. wishes to thank Professor Scherrer for offering this research internship opportunity as well as all the guidance and various pieces of advice that made this research productive. This work was supported by NASA contract NAS5-02139 (HMI) and NSF grant AGS 1836370 (WSO). MDI data provided by the SOHO/MDI consortium. SOHO is a project of international cooperation between ESA and NASA. The data shown inclination data shown in Figure 2 is available at https://purl.stanford.edu/yq160kn5895.

ORCID iDs

Philip H. Scherrer https://orcid.org/0000-0002-6937-6968

References

Cameron, R. H., Duvall, T. L., Schüssler, M., & Schunker, H. 2018, A&A, 609, A56
Duvall, T. L. J., Scherrer, P. H., Svalgaard, L., & Wilcox, J. M. 1979, SoPh, 61, 233
Howard, R., & Labonte, B. J. 1980, ApJL, 239, L33
Lo, L., Hoeksema, J. T., & Scherrer, P. H. 2010, in ASP Conf. Ser. 428, SOHO-23: Understanding a Peculiar Solar Minimum, ed. J. T. Hoeksema, J. L. Kohl, & S. R. Cranmer (San Francisco, CA: ASP)
Ma, W., & Scherrer, P. H. 2016, Signs of Cycle 25 Seen in the Surface Toroidal Field, http://hmi.stanford.edu/hminuggets/?p=1657
Pesnell, W. D., Thompson, B. J., & Chamberlin, P. C. 2012, SoPh, 275, 3
Scherrer, P. H., Bogart, R. S., Bush, R. I., et al. 1995, SoPh, 162, 129
Scherrer, P. H., Schou, J., Bush, R. I., et al. 2012, SoPh, 275, 207
Scherrer, P. H., Wilcox, J. M., Svalgaard, L., et al. 1977, SoPh, 54, 353
Shrauner, J. A., & Scherrer, P. H. 1994, SoPh, 153, 131
Snodgrass, H. B. 1985, ApJ, 291, 339
Snodgrass, H. B. 1987, SoPh, 110, 35
Ulrich, R. K. 1993, in ASP Conf. Ser. 40, IAU Colloq. 137: Inside the Stars, ed. W. W. Weiss & A. Baglin (San Francisco, CA: ASP)
Ulrich, R. K., & Boyden, J. E. 2005, ApJL, 620, L123
Ulrich, R. K., Evans, S., Boyden, J. E., & Webster, L. 2002, ApJS, 139, 259